Piezoelectric Soft Robots for Inchworm Crawling and Jumping Optimized with Weight Asymmetry

Zhiwu Zheng, Hsin Cheng, Prakhar Kumar, Yenan Chen,
Sigurd Wagner, Minjie Chen, Naveen Verma and James C. Sturm

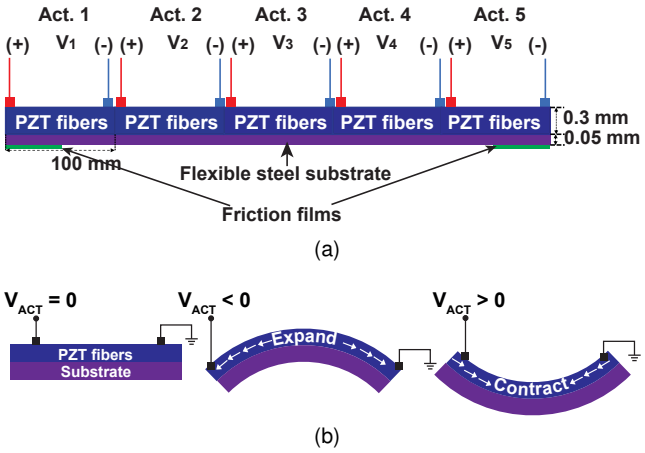

Fig. 1. (a) Cross-section of the demonstrated five-actuator soft robot prototype, 500 mm long and 20 mm wide. A high friction film of 50 mm length is applied on the underside of each end. (b) Mechanism of bending, based on piezoelectric effect, whereby an actuator unit curves concave down (up) due to expansion (contraction) under negative (positive) actuator voltage.

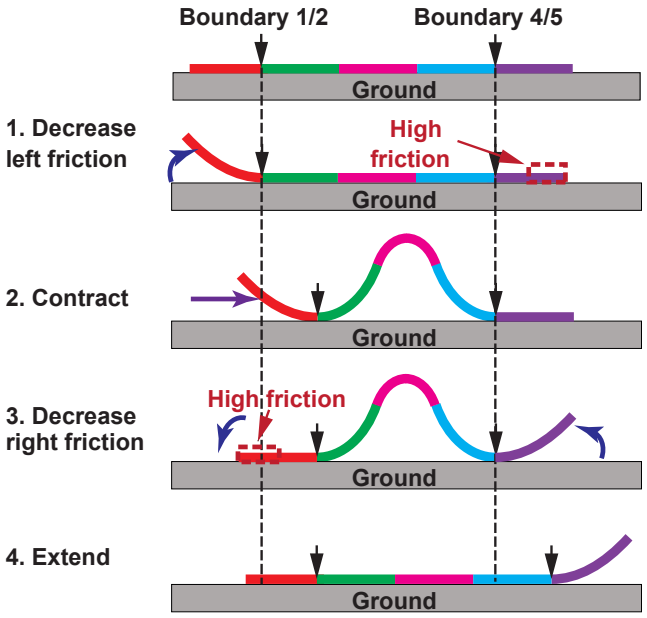

Fig. 2. Inchworm motion of "contract" and "extend" cycles in 4 steps. The high-friction films at the ends are raised and lowered on opposite ends to create a friction asymmetry to generate motion. Each piezoelectric actuator in the five-actuator robot is shown in by a different color.

Soft robots have gathered great interest as of their rich range of shapes and motions, compared to traditional rigid robots. Particularly, electrostatic soft robots have small form factors and fast response speed [2]. However, statics and dynamics, especially when interacting with the environment, pose significant challenges for robust modeling necessary for robot design and control. Most recent work focuses on pneumatic [3], shape-memory, or motor tendon soft robots [4], [5]. Scalable approaches for electrostatic soft robots have been limited. With some examples on single-actuator robot [2] and a roller made of dielectric elastomer actuators [6]. Studies on dynamics of multi-actuator piezoelectric soft robots have been limited.

This work demonstrates a five-actuator piezoelectric soft robot that is capable of crawling and jumping. It includes nearly-static "inchworm" motions, and jumping (in vertical as well as vertical and horizontal directions). These motions exhibit complex non-linear behavior.

Optimization of the horizontal motion is further explored experimentally. We found that with specific voltage sequence and weight distribution by adding external loads, the robot can move up to ∼6 cm/s.

The robot consists of five 100-mm-long 20-mm-wide 300-µm-think piezoelectric devices bonded to a single 50-µm-thick layer of steel foil (side view shown in Fig. 1a). A 50-mm-long frictional film is bonded to each end of the robot. The robot rests on the ground and is driven by five external voltages connected by thin compliant wires.

Fig. 1b shows bending mechanism of a single actuator bonded onto a steel foil. When negative (positive) voltage is applied, the piezo device expands (contracts), while the steel foil, due to its high strength, remains fixed in its length. As a result, the whole structure bends concave down (up).

Fig. 2 shows a schematic view of a five-actuator robot structure used for experimental demonstration in this work. Inchworm-like motion is possible by exploiting asymmetry in friction alternating between its two ends: in step 1, actuator #1 (left end) is turned on to raise it to reduce friction on the left end; in step 2, actuators #2, #3, and #4 are turned on; in step 3, actuator #1 is turned off and actuator #4 is turned on, to change the end with friction; in step 4, actuators #2, #3, and

This work was supported by the Semiconductor Research Corporation (SRC), DARPA, Princeton Program in Plasma Science and Technology, and Princeton University. This abstract briefly describes a paper that has been accepted to the 2022 IEEE International Conference on Robotics and Automation (ICRA) [1], and part of a paper that is under review for the 2022 IEEE/RSJ International Conference on Intelligent Robots and Systems (IROS2022). *(Corresponding author: Zhiwu Zheng)*

The authors are with the Department of Electrical and Computer Engineering, Princeton University, Princeton, New Jersey 08544, U.S.A. (e-mails: zhiwuz@princeton.edu; hsin@princeton.edu; prakhark@princeton.edu; yenanc@zju.edu.cn; wagner@princeton.edu; minjie@princeton.edu; nverma@princeton.edu; sturm@princeton.edu). Yenan Chen is currently with Hangzhou Global Scientific and Technological Innovation Center at ZheJiang University.

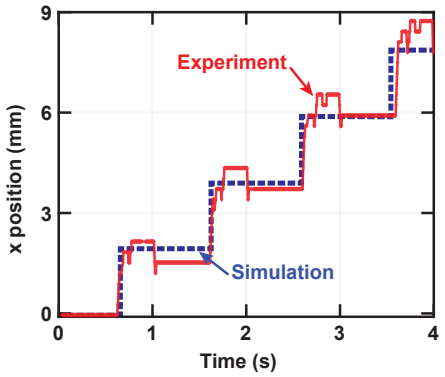

Fig. 3. Experimental validation of rightward inchworm-motion robot simulation.

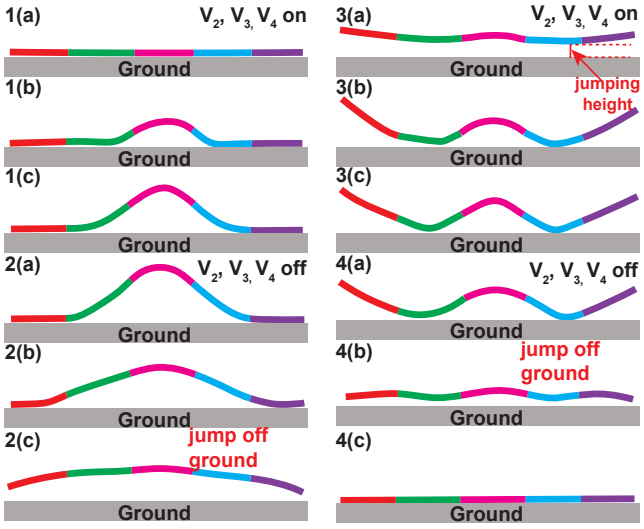

Fig. 4. Robot jumping observed in experiments (from high-speed cameras) due to alternating turning V_2, V_3 and V_4 on and off. The frequency of the voltage cycling is 14 Hz. The whole robot can jump off the ground at least 7.5 mm high, referred as "jumping height" (in step 3(a)).

#4 are turned off. The robot moves at low speed by holding a desired end fixed on the ground and then contracting/extending through its central three actuators.

Fig. 3 demonstrates rightward inchworm motion of the robot (as shown in Fig. 2). Different actuators turn on at different steps. The turn-on voltages are: $V_1 = 300$ V, $V_2 = 300$ V, $V_3 = -1500$ V, $V_4 = 300$ V, and $V_5 = 300$ V. The robot moves cycle by cycle. Each cycle takes 1 s, giving overall horizontal robot motion of 1.9 mm per cycle and average speed of 1.9 mm/s. This is again in good agreement with the simulations. Details about simulation approaches can be found in our previous work [1].

In-place jumping is a 2-phase symmetric motion, where first the middle three actuators are turned on simultaneously to lift the central section, followed by turning them off. Fig. 4 illustrates experimentally-observed shapes (from high-speed cameras) over two driving periods.

The vertical momentum of the midsection is generated by turning them ON (Step 1) and transmitted to other parts along the length of the robot (Step 2) when they are turned

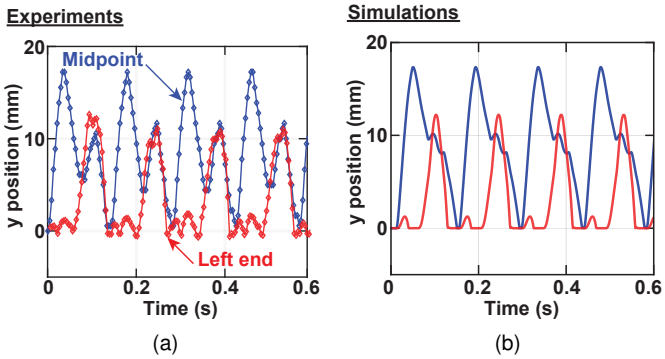

Fig. 5. Time-domain movement of the robot from (a) experiments and (b) simulations, based on tracking the vertical positions of two representative points on the robot (blue line is robot midpoint, red line is robot end point).

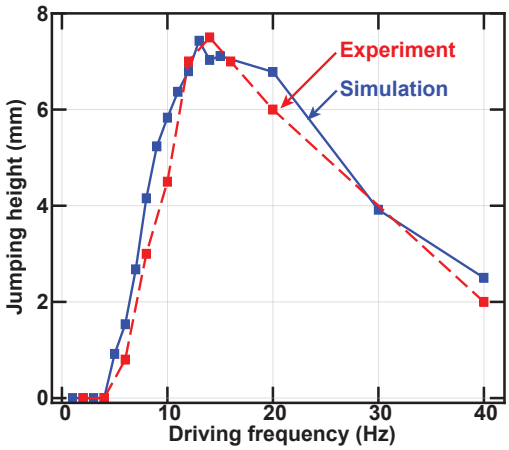

Fig. 6. Jumping height vs. driving frequency using three motors per actuator in simulations, showing excellent agreement between simulations and experiments.

OFF, with all parts are lifted off the ground. Steps 3 and 4 repeat Steps 1 and 2. However, as the robot is off the ground at the beginning of Step 3, the robot's motion is different from Steps 1 and 2. The motion is highly non-linear, as the period of the maximum height is twice that of the driving sequence. Fig. 5a shows experimental results of time-domain movement of the midpoint and the end. Simulation (Fig. 5b) shows great agreement with the experiment, accurately capturing the motion's multiple unusual features. Fig. 6 shows frequency dependency of the experimental and simulated maximum jumping height off the ground (measured at the robot's lowest point) during a full cycle. The robot can jump as high as ~8 mm. Remarkably good agreement is achieved between simulations and experiments without any curve-fitting parameters.

The symmetric applied voltages in the previous section lead to no left/right net motion, as expected. We now further explore frequency-dependent characteristics of the robot for the inchworm sequence of steps. The driving frequency of the control voltages is swept from low frequencies to high frequencies while maintaining the inchworm control-voltage sequencing (Fig. 7). Inchworm motion (as in Fig. 3) is observed at low frequencies (up to 3 Hz). Beyond

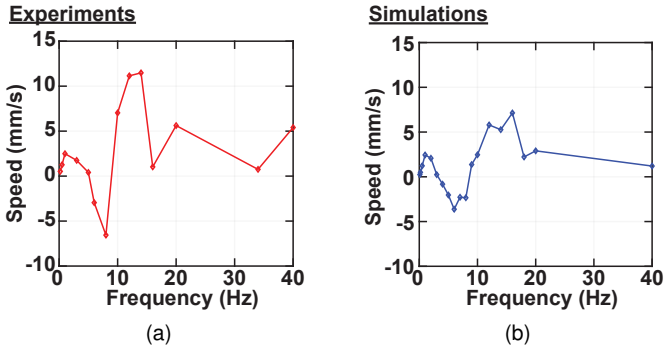

Fig. 7. Robot rightward speed as a function of frequency from (a) experiments and (b) simulations. Input voltage sequences are the same as the inchworm motion, but with a higher frequency. Simulation and experimental results agree qualitatively, including a reversal of direction at ~8 Hz, and maximum rightward speed at ~14 Hz.

this, a reversal in the direction of motion is observed, maximized at a frequency of 8 Hz for -7 mm/s. Further beyond this, at even higher frequencies, the robot is observed to move rightward again, with a peak rightward speed at 14 Hz of 12 mm/s. These frequency-dependent motions, including reversal of the movement direction, are corroborated qualitatively by the simulation, and they are currently being investigated by analyzing different vibration modes caused by different frequencies. We expect to obtain closer agreement by introducing accurately measured friction coefficients and damping factors.

We further explore optimization of the horizontal motion by special voltage sequence and weight distribution (by adding external loads), as well as elastic components at the bottom. Fig. 8a shows the experimental setup. Five B-shape hollow foam feet are attached for storing and converting elastic energy to boost the motion. A simple weight non-uniformity is added, which we observe to cause frequency-dependent horizontal motion. A 3-gram weight is attached at the midpoint of the robot's actuator #1, and another 13-gram weight is attached at the end of actuator #4 (Fig. 8a). All the actuators are cycled on and off is while sweeping the driving frequency. Here, the robot's axial speed and direction change significantly with frequency. Fig. 8b shows that: as frequency increases, the robot moves leftward, up to -6.1 mm/s at 8 Hz; changes direction to move rightward, up to 25 mm/s at 16 Hz; and finally moves leftward again, up to -54 mm/s at 23 Hz. Figs. 8c and 8d plot the robot's horizontal positions versus time for two different driving frequencies. The robot moves rightward by 25 mm/s when driven at 16 Hz and leftward by -54 mm/s when driven at 23 Hz.

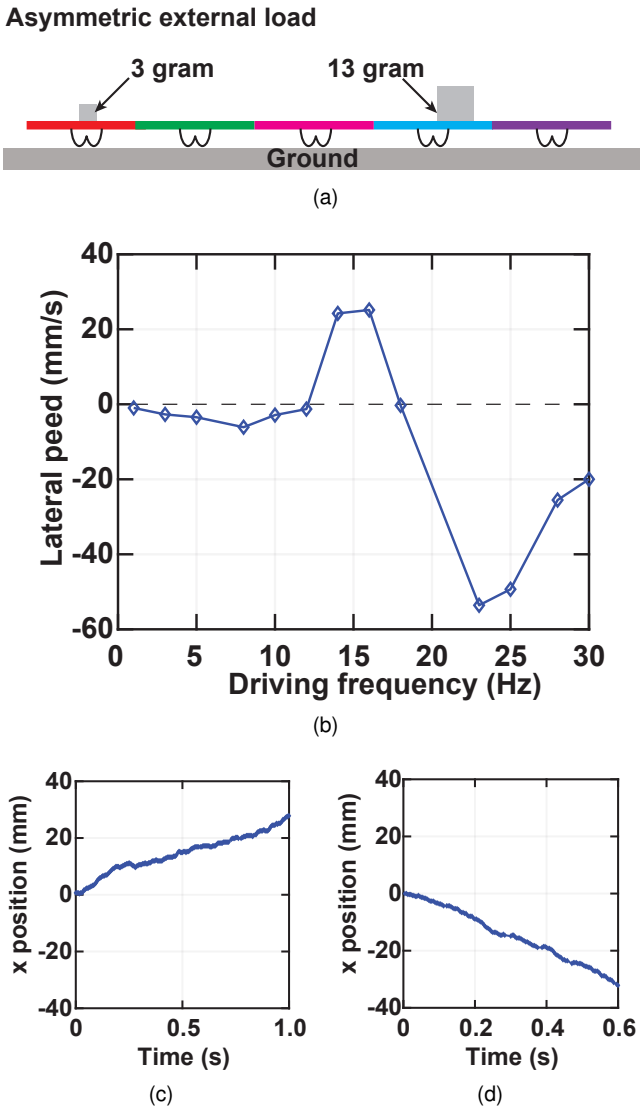

Fig. 8. Robot with non-uniform loading. (a) Robot setup with a 3-gram weight on the middle of actuator #1 and 13-gram weight on actuator #4. (b) Frequency dependence of the robot's axial speed, with the non-uniform setup in Fig. 8a. (c) Robot rightward motion of 25 mm/s, when driven at 16 Hz. (d) Robot leftward motion of -54 mm/s, when driven at 23 Hz.

References

[1] Z. Zheng, P. Kumar, Y. Chen, H. Cheng, S. Wagner, M. Chen, N. Verma, and J. C. Sturm, "Scalable Simulation and Demonstration of Jumping Piezoelectric 2-D Soft Robots," feb 2022. [Online]. Available: http://arxiv.org/abs/2202.13521

[2] Y. Wu, J. K. Yim, J. Liang, Z. Shao, M. Qi, J. Zhong, Z. Luo, X. Yan, M. Zhang, X. Wang, R. S. Fearing, R. J. Full, and L. Lin, "Insect-scale fast moving and ultrarobust soft robot," *Science Robotics*, vol. 4, no. 32, p. eaax1594, jul 2019. [Online]. Available: https://robotics.sciencemag.org/lookup/doi/10.1126/scirobotics.aax1594

[3] C. Della Santina, R. K. Katzschmann, A. Biechi, and D. Rus, "Dynamic control of soft robots interacting with the environment," in *2018 IEEE International Conference on Soft Robotics (RoboSoft)*. IEEE, apr 2018, pp. 46–53. [Online]. Available: https://ieeexplore.ieee.org/document/8404895/

[4] W. Wang, J.-Y. Lee, H. Rodrigue, S.-H. Song, W.-S. Chu, and S.-H. Ahn, "Locomotion of inchworm-inspired robot made of smart soft composite (SSC)," *Bioinspiration & Biomimetics*, vol. 9, no. 4, p. 046006, oct 2014. [Online]. Available: https://iopscience.iop.org/article/10.1088/1748-3182/9/4/046006

[5] T. Umedachi, V. Vikas, and B. A. Trimmer, "Softworms : the design and control of non-pneumatic, 3D-printed, deformable robots," *Bioinspiration & Biomimetics*, vol. 11, no. 2, p. 025001, mar 2016. [Online]. Available: https://iopscience.iop.org/article/10.1088/1748-3190/11/2/025001

[6] W.-B. Li, W.-M. Zhang, H.-X. Zou, Z.-K. Peng, and G. Meng, "A Fast Rolling Soft Robot Driven by Dielectric Elastomer," *IEEE/ASME Transactions on Mechatronics*, vol. 23, no. 4, pp. 1630–1640, aug 2018. [Online]. Available: https://ieeexplore.ieee.org/document/8365835/